STRESS DISTRIBUTION DURING CAVITATION OF COMPACT GRAPHITE IRON

Newton Kiyoshi Fukumasu
Surface Phenomena Laboratory, Department of Mechanical Engineering, Polytechnic School of the University of São Paulo
Av. Prof. Mello Moraes 2231, 05508-900 São Paulo, Brazil
newton.fukumasu@poli.usp.br

Paula Luci Pelegrino
Surface Phenomena Laboratory, Department of Mechanical Engineering, Polytechnic School of the University of São Paulo
Av. Prof. Mello Moraes 2231, 05508-900 São Paulo, Brazil
paula.pelegrino@poli.usp.br

Edison Gustavo Cueva
Surface Phenomena Laboratory, Department of Mechanical Engineering, Polytechnic School of the University of São Paulo
Av. Prof. Mello Moraes 2231, 05508-900 São Paulo, Brazil
gustcg@usp.br

Roberto Martins Souza
Surface Phenomena Laboratory, Department of Mechanical Engineering, Polytechnic School of the University of São Paulo
Av. Prof. Mello Moraes 2231, 05508-900 São Paulo, Brazil
roberto.souza@poli.usp.br

Amilton Sinatora
Surface Phenomena Laboratory, Department of Mechanical Engineering, Polytechnic School of the University of São Paulo
Av. Prof. Mello Moraes 2231, 05508-900 São Paulo, Brazil
sinatora@usp.br

Abstract. *The wear behavior of compact graphite iron (CGI) was studied both experimentally and based on a finite element analysis of the stresses developed during cavitation wear tests. During the experimental portion of this work, the compact graphite iron was submitted to thermal treatments of annealing and quenching to modify the original strength and hardness. Three levels of hardness were then analyzed: (i) low hardness – treated CGI with ferritic matrix; (ii) medium hardness – original CGI with pearlitic matrix and (iii) high hardness – treated CGI with martensitic matrix. The three different materials were later subjected to cavitation erosion tests in a laboratory equipment. In terms of the numerical analysis, the software ABAQUS was used and meshes were generated with the help of the OOF simulation package, developed at the National Institute of Standards and Technology (NIST). Consistent with the experimental procedure, the main parameters analyzed in the simulations were the yield strength and work hardening coefficient of the CGI matrix. Good agreement was obtained when numerical and experimental analyses were compared. Both methods indicated that the hardness of the matrix affects the wear behavior of the CGI. Additionally, the finite element results allowed the observation of stress concentrations in the cast iron matrix, as a result of the presence of graphite flakes.*

Keywords*: Compact graphite iron, cavitation, residual stresses, Finite element modeling*

1. Introduction

According to Liu (1981), Hrusovsky and Wallace (1985) and Guesser and Guedes(1997), due to a good combination of mechanical and thermal properties, compact graphite iron (CGI) is largely manufactured into mechanical components, such as ingot molds, cylindrical heads, exhaust manifold brake components, hydraulic valve bodies and vehicular engine blocks. In some of these applications, Iwai *et. al.* (1983) mention that the component is exposed to cavitation-erosion conditions, in particular, when the components are in contact with high temperature liquids; for example, in hydraulic machines or vehicular engines.

Several woks on the processing of cast iron (Liu, 1981, Hrusovsky and Wallace 1985, Guesser and Guedes, 1997, Iwai *et. al.*, 1983 and Dunks and Turner, 1981) have looked into the optimization of mechanical characteristics such as toughness and fatigue and wear resistance. However, these works indicate an enormous variation of these characteristics as a function of, mainly, chemical composition, type of metallic matrix and morphology of graphite. It is also known (Tomlinson and Talks, 1990) that the graphite flakes work as stress concentrators and that their effect is more critical when the irons have graphite with lamellar morphology.

Recent works on steel and white cast iron (Martins *et. al.*, 2004 and Serantoni, 2003) show results of stress distribution when the materials are subjected to temperature variations and wear processes (Fukumasu *et. al.*, 2004 and Cuppari *et. al.*, 1999). The objective of this work is to enhance the comprehension in this area, by using the finite

elements method (FEM) to analyze the influence of hardness over the stress distribution developed during cavitation wear tests of CGI.

2. Material and methods

2.1 Material

Table 1 presents the chemical composition, the Brinell hardness (HB) and the ultimate tensile strength (UTS) of the CGI studied in this work, in the as cast (original) condition. The mechanical properties presented in Table 1 were evaluated in a previous work (Cueva *et. al.* 2003), following standard procedures for these types of analyses. Table 2 presents the microstructural characteristics of the original CGI, which consisted basically of pearlite, ferrite, vermicular graphite and traces of spherical graphite. The average value of the graphite aspect ratio L/D (L = length and D = width) was 8 ± 2.

Table 1. Chemical composition (wt%) and mechanical properties of the compact graphite iron studied in this work.

C	Si	Mn	P	S	Ti	Hardness (HB)	UTS (MPa)
3.6	2.1	0.5	0.04	0.02	<0,001	215 ± 5	460

Thermal treatments were applied to the CGI with the characteristics presented in Table 2. These treatments were: (i) Annealing – austenitization at 900 ^{o}C for 30 minutes and cooling until 700 ^{o}C at a cooling rate of 40 ^{o}C/h, temperature hold at 700 ^{o}C for 2 hours and final cooling to room temperature inside the furnace and (ii) Quenching – austenitization at 900 ^{o}C for 30 min and quenching in water until room temperature.

Instrumented indentation tests were conducted in the original and treated CGI specimens, in order to investigate the mechanical properties of each phase separately. In instrumented indentation, the specimen is submitted to a load/unloading cycle, in which the applied load and the penetration depth are continuously monitored. In this work, the analysis of indentation load-displacement curves allowed the calculation of hardness, elastic modulus (E) and strain hardening exponent (n). Calculations were based on a procedure described by Cuppary (2002). Instrumented indentation analyses were conducted in a FISCHERSCOPE HV 100 with a Vickers indenter and a total of twenty impressions, with a load of 100 mN, was used to evaluate the mechanical properties of each phase. For the original CGI (pearlitic matrix), the results from the instrumented indentation experiments are presented in Table 2. Similar procedures were used to analyze the irons that were thermally treated and these results are shown in Tables 3 and 4.

Table 2. Microstructural characteristics of compact graphite cast iron studied in this work.

	Graphite	Pearlite	Ferrite
Volume (%)	11 ± 2	82 ± 2	7 ± 2
Type	80% IIIA5 - 20% IA6		
L/D	8 ± 2		
Hardness (HV)	60 ± 10	300 ± 10	188 ± 25
Young's modulus – E (GPa)	23 ± 3	189 ± 5	168 ± 20
Yield strength - σ_y (MPa)	125 ± 30	587 ± 13	316 ± 50
Strain hardening exponent - n	0.155 ± 0.04	0.136 ± 0.005	0.200 ± 0.009

Table 3. Microstructural characteristics of treated CGI.

Condition	%vol. Graphite	%vol. Ferrite	%vol. Pearlite	%vol. Martensite	Hardness HV30
Cast iron - original	11	7	82	-	215 ± 10
Ferritized	11	71	18	-	180 ± 10
Quenched	11	-	-	89	615 ± 10

Table 4. Mechanical properties of martensite.

	Martensite
Hardness (HV)	800 ± 50
Young's modulus – E (GPa)	191 ± 8
Strain hardening exponent - n	0

2.2 Wear test

In this work, cavitation tests were conducted in a vibratory device (TELSONICSG1000), following an ASTM Standards (1992). Specimens were held stationary throughout the tests at a distance of 0.5 mm from the vibrating horn (Figure 1). The frequency and vibration amplitude were kept constant at 20 kHz and 40 μm, respectively.

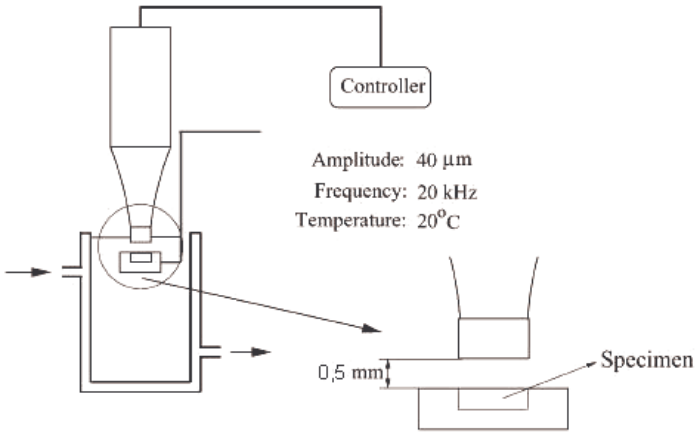

Figure 1. Schematic of the cavitation erosion tests.

All tests were conducted in distilled water at a constant temperature of 20 °C. The tests were interrupted at regular time intervals in order to evaluate the evolution of mass loss along each test, which had total durations of 300 minutes. After each interval, specimens were cleaned using ultra-sound and the mass loss was then determined using an analytical scale. During these interruptions, the worn surfaces were observed under an optical microscope, in order to identify the wear mechanisms. At least three tests were carried out in specimens of each level of hardness studied.

2.3 Finite element modeling

Finite element method simulations were conducted with the ABAQUS software. The mesh was generated through the software "ppm2oof", developed at the National Institute of Standards and Technology – NIST. This software allows the generation of a two-dimensional mesh, where plane strain triangular elements reproduce the different phases observed in digitalized micrographs (Figure 2). Each simulation was conducted such that the graphite flake shown in Figure 2 was considered to be embedded in each of the matrices analyzed: pearlitic, ferritic and martensitic. The mesh was more refined in certain regions, in order to increase the accuracy of contact conditions and microstructural features. The loading conditions used in the simulations were based on the assumption that the cavitation shock waves stresses the specimen in the direction perpendicular to the surface, resulting in strains in the orthogonal directions (Cuppari, 2002). Roughly, these orthogonal strains may be obtained through Eq. (1), where σ_{33} is the stress applied to the specimen during the test and ν is the Poisson ratio. More accurate calculations should consider both elastic and plastic contributions for ε_{11} and ε_{22}. The intensity of the shock waves generated during the cavitation tests are not known accurately. Okada et al. (1989) presented a compilation of literature results, combining both simulations and experimental results. Based on this compilation, a value of 1GPa was assumed for the σ_{33} stress. The Poisson ratio was assumed to be equal to 0.33. Once the values of ε_{11} and ε_{22} were calculated, the system was loaded by imposing these strains to the meshes generated based on Figure 2.

$$\varepsilon_{11} = \varepsilon_{22} = -0{,}5 \times \varepsilon_{33} \text{ and } \varepsilon_{33} = \frac{\nu.\sigma_{33}}{E} \quad (1)$$

During the simulations, it was assumed that matrix (pearlite, ferrite or martensite) and graphite presented an isotropic behavior and, for CGI, that the interface between both phases was perfect, such that no separation was allowed along the matrix/graphite interface. Pearlite and ferrite phases were considered to be elasto-plastic and martensite was assumed to be only elastic. In all cases, large strains were allowed without fracture.

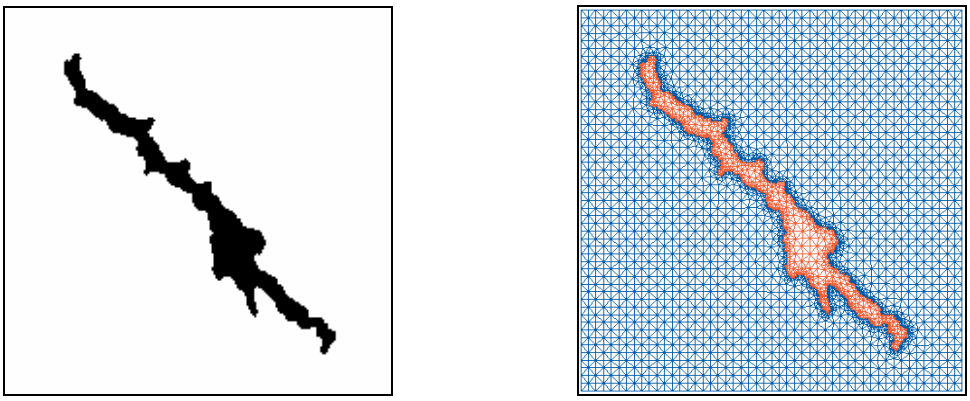

(a) (b)

Figure 2. Overview of the meshes used to simulate the stresses developed during the cavitation tests. (a) morphology of real graphite flake, digitalized and (b) mesh created for the graphite flake and the metallic matrix.

3. Results and discussions

3.1. Wear

Figure 3 presents the curves of cumulative mass loss as a function of time. In the figure, the slope of the curves change throughout the test, which indicates that, independent of matrix hardness, the wear rate is not uniform along the test. Three different regions may be defined for the curves presented in Figure 3: I) up to 40 min; II) from 45 to 120 min and III) from 130 min.

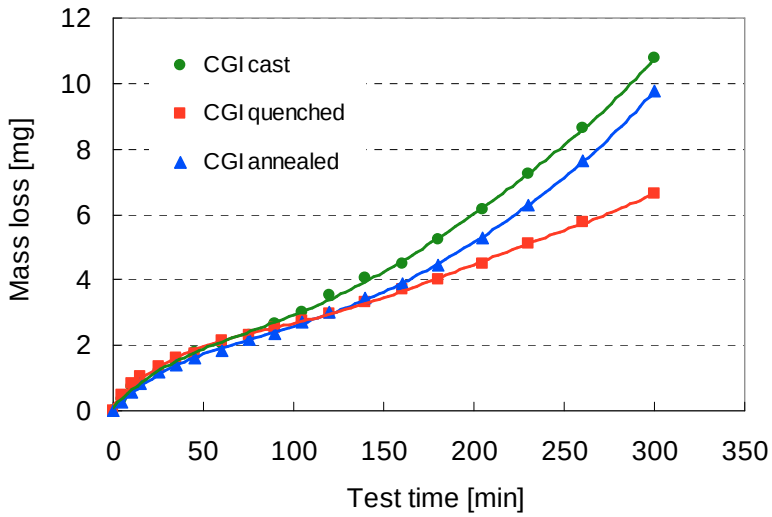

Figure 3. Cumulative mass loss of compact graphite iron as a function of test time and hardness: CGI cast – original cast iron; CGI quenched – martensitic matrix and CGI annealed – ferritic matrix.

In **Region I**, mass loss curves are similar, although the hardest specimen presents a mass loss slightly higher than the others, followed by the material with the intermediate matrix hardness and the material with the softest matrix. The high wear rate observed in the beginning of the test is mainly attributed to the removal of graphite, to the damage at regions close to the cavities left by graphite and to surface pitting (Figure 4).

In **Region II**, the wear rate decreases significantly and becomes uniform for all materials. In this region, it is possible to observe that the harder CGI becomes more wear resistant, followed by the material with the softest matrix and, finally, by the material with intermediate hardness. Figure 4 indicates that, during this period, the matrices are further worn out by pitting and in regions close to the cavities left by graphite. Wear occurs mainly in areas where the graphite flakes are more acute, which result in the widening of the worn areas.

In **Region III**, a clear difference was observed in the mass loss curves presented in Figure 3, further expanding the wear trends initiated in Region II. In Region III, wear is no longer limited to the cavities left by graphite and extends through the entire surface (Figure 4).

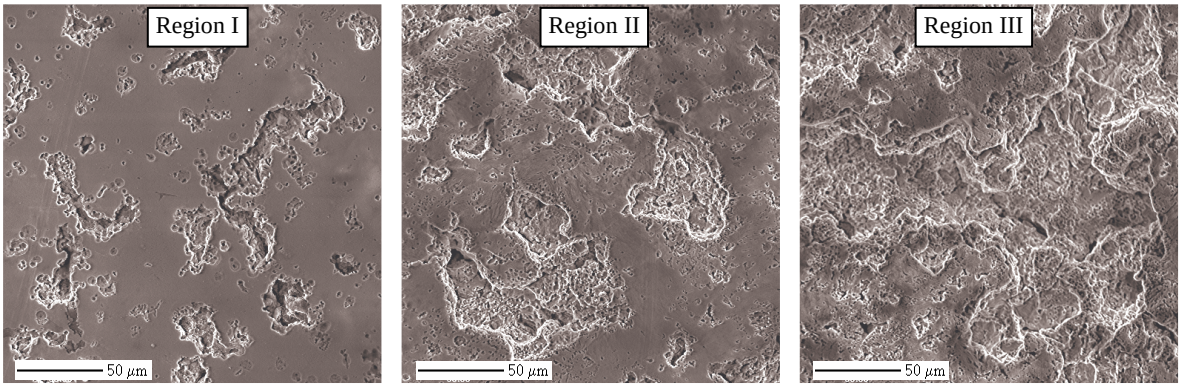

Figura 4. Wear evolution (CGI, as cast). Region I: after 10 min of cavitation test; Region II: after 60 min of cavitation test and Region III: after 150 min of cavitation test.

The wear behavior of the CGI with ferritic matrix is not in agreement with literature works on the wear of steels. According to Hansson and Hansson (1996) continuous ferritic microstructures provide the worst wear resistance to cavitation. That behavior is attributed to the easy removal of ferrite from the boundary of carbides, which would also be removed due to the lack of support from the matrix. Therefore, thermal treatments are usually recommended towards the formation of martensite, or bainite, which improve matrix strength and reduce cavitation wear.

3.3. Finite Element Modeling

The FEM analyses conducted considering the materials with different hardness levels indicated that stresses were intensified at the ends of the graphite flakes and in positions where the surface of the flake was not uniform. Figure 5 presents the distribution of maximum principal stresses for the three materials at the moment when the highest strain was applied to the mesh. In this figure, it is possible to observe that the maximum principal stresses are tensile over the entire surface and that stresses are lower in the specimen with the lowest hardness, followed by the specimen with intermediate hardness and, finally, by the hardest specimen. The high stress values observed for the pearlitic and martensitic matrices appear since the stresses in the matrices were allowed to increase indefinitely without the occurrence of fracture. Although these results may be qualitatively correct, such high stress values are not expected to occur in practice.

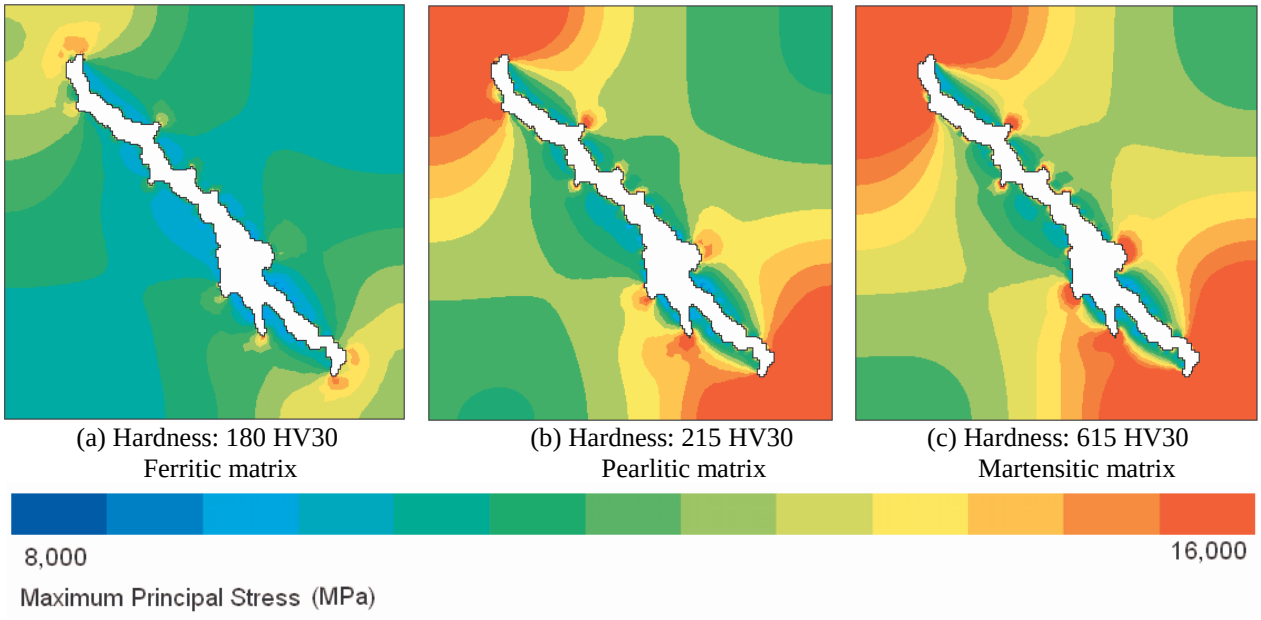

Figura 5. Distribution of maximum principal stresses around a graphite flake embedded in different matrices. Application of maximum strain: (a) ferritic matrix; (b) pearlitic matrix and (c) martensitic matrix.

The stress distributions shown in Figure 5 may be explained based on the mechanical properties attributed to the matrix of each specimen. The lower yield strength of ferrite (Table 2) results in higher levels of plastic deformation and, consequently, in an improved ability to absorb the energy from cavitation and to distribute this energy uniformly through its volume (Figure 5a). The energy absorbed by pearlite (Figure 5b) occurs mainly elastically and, therefore, pearlite is unable to distribute the cavitation energy as efficiently as ferrite. The martensitic matrix (Figura 5c) presents the highest levels of maximal principal stresses at maximum load. In this work, martensite was considered to be only elastic, which is in agreement with its usual brittle behavior. Therefore, this specimen is also unable to distribute the applied load throughout the specimen volume and stresses become concentrated in preferential sites such as the graphite ends.

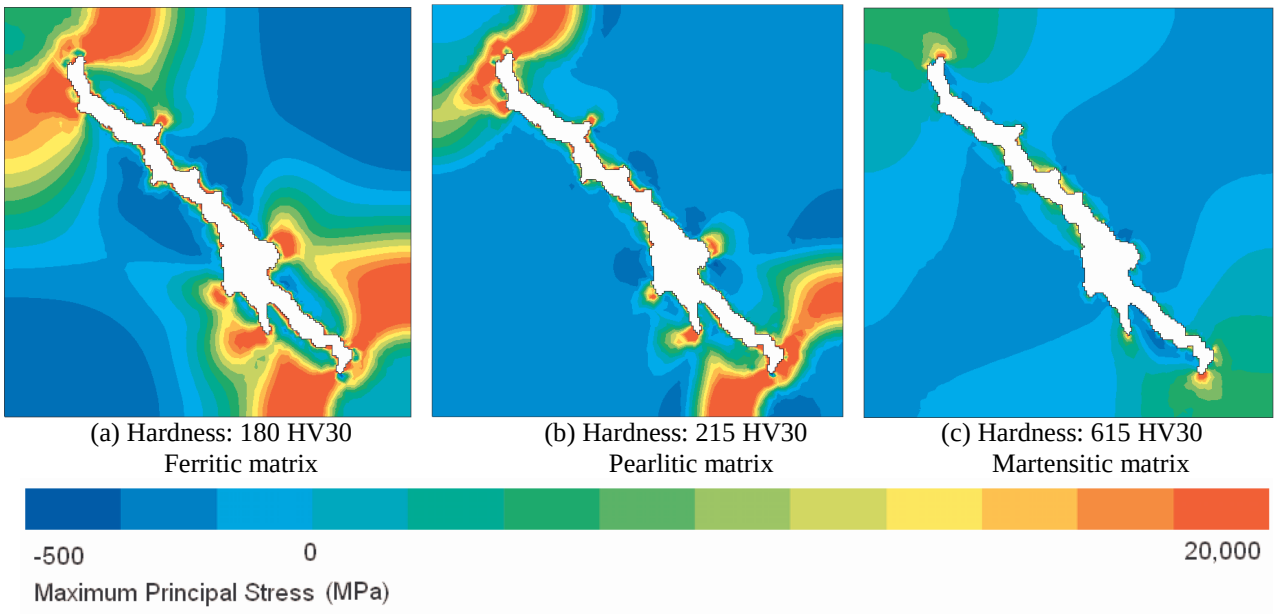

Figure 6. Distribution of minimum principal stresses around a graphite flake embedded in different matrices. Residual stresses after strain removal: (a) ferritic matrix; (b) pearlitic matrix and (c) martensitic matrix.

Different stress distributions were obtained after the strains imposed to the meshes were removed. Figure 6 presents the distribution of residual (after strain removal) maximum principal stresses for the three cases studied in this work. It is possible to observe that these stresses are predominantly compressive in all cases, except for the regions close to the graphite ends and flake irregularities. These locations were those for which the stress concentrations were higher during the loading portion of straining cycle.

Figures 6a and 6b indicate that the ferritic and pearlitic matrices are subjected to the highest degrees of tensile residual stresses. This observation presents a possible explanation for the highest wear resistance of the CGI with martensitic matrix. Since cavitation is associated with several loading cycles, it is possible to expect that the pearlitic and ferritic matrices will become increasingly subjected to tensile stresses, favoring an increase in mass loss throughout the experiments. The differences observed experimentally for these two materials are possibly associated with the fracture toughness. Since residual stress distributions are similar for these two materials, more damage would be expected in the material with the lower fractures toughness, which is pearlite.

In the case of the cast iron with martensitic matrix, Figure 6 indicates that there are essentially no residual stresses along the matrix. Considering that residual stresses appear whenever there are differential plastic deformations in a material, this result is explained based on the elastic behavior imposed to the martensite. In fact, the regions presenting residual stresses different from zero are a result of the plastic deformation of graphite, which was assumed to present an elastic-plastic behavior.

The mechanical properties of the matrices significantly altered the cavitation behavior of the CGI studied in this work. Higher values of hardness were observed with the martensitic matrix, which experimentally presented the highest wear resistance. The numerical results have shown that, although this matrix provides an increase in the tensile stresses during the loading portion of the straining cycle, these stresses may be almost entirely removed during unloading. Therefore, this type of matrix would present an essentially elastic behavior during the experiments, limiting the damage to pitting areas and to areas where stress concentration would occur due to the removal of graphite flakes.

4. Conclusions

In the conditions proposed for this work, it was observed that:

- The cavitation wear of compact graphite iron, independent of hardness, occurs in three stages: I) removal of graphite and pit; II) Fracture along the edges of the cavities left by graphite removal and pit and III) wear over the entire surface.
- Stress concentration occurs during the cavitation wear of compact graphite iron, especially at the ends of graphite flakes and at irregularities along the surface of the flake.
- When the applied load is removed, regions with the highest tensile stresses become subjected to residual compressive stresses.
- Tensile residual stresses were predominant in the compact graphite iron with pearlitic and ferrítica matrix, in comparison with those with martensitic matrix.
- Good agreement was observed when the stresses calculated in the finite element analysis were compared with the wear rates measured during cavitation tests.

5. Acknowledgements

The authors would like to acknowledge Indústria de Fundição Tupy Ltda. for the donation of the cast iron, and the financial support provided by the State of São Paulo Research Foundation (FAPESP), though process nº 03/06517-3, and the National Council for Scientific and Technological Development (CNPq), through process 550177/2003-5 RHAE.

6. References

ANNUAL BOOK OF ASTM STANDARDS, 1992Standard Test methods for Cavitation Erosion Using Vibratory Apparatus, G32-92.

Cueva, G., Guesser, W.L., Sinatora, A., Tschipstchin, A.P. Wear resistance of cast irons used in brake disc rotors, Wear, v. 255, 2003, p. 1256–1260.

Cuppari, M. G. V., Sinatora, A., Wischnowski, F., Tanaka, D. K. Correlation Between Microstructure And Cavitation-Erosion Resistance Of High-Chromium Cast Steels - Preliminary Results. Wear, v. 225, 1999, p. 519 - 524,.

Cuppari, M. G. V., Relação entre microestrutura e resistência à cavitação de ligas fundidas baseadas no sistema quaternário Fe-Cr-C-Ni. Tese de Doutorado. Escola Politécnica da Universidade de São Paulo. 2002.

Dunks, C.M., Turner, K.B., Production of compacted graphite iron casting for brake systems. AFS Transactions, v. 89, 1981, p. 575 – 586.

Fukumasu, N., Pelegrino, P. L., Cueva, G., Souza, R. M., Sinatora, A. Análises da distribuição de tensões na microestrutura durante a cavitação de ferros fundidos vermiculares. ANAIS: 59º. Congresso ABM 2004.

Guesser, W. L. , Guedes L.C. Desenvolvimentos recentes em ferros fundidos aplicados à indústria automobilística. IX Simpósio de Engenharia Automotiva, AEA. São Paulo, Ag.1997.

Hansson, C., Hansson, I. L.H. Cavitation Erosion. In ASM Hanbook. Friction, Lubrication and Wear Technology, v. 18, 1996, p. 214 - 220.

Hrusovsky, J. P., Wallace, J. F. Effect of Composition on Solidification Compact Graphite Iron. AFS Transaction. v. 93, 1985, p. 55 - 72

Iwai, Y., Okada, T., Hammitt, F.G. Effect of temperature on the cavitation erosion of cast iron. Wear, v. 85, 1983. p. 181-191.

Liu, P.C., Loper, C.R. Jr., Kimura, T., Pan, E. N. Observations on the graphite morphology of compact graphite cast iron. AFS Transactions, v.89, 1981, p. 65 – 78.

Martins A., Souza, R. M, Da Silva C. S. Redução de tensões térmicas mediante alteração de propriedades das fases um estudo computacional. ANAIS: 12º. SIICUSP, 2004.

Okada, T., Iwai, Y., Awazu, K A study of cavitation bublle collapse pressures and erosion. Part I A method for measurement of collapse pressures. Wear, v. 133, 1989, p. 219 – 232.

Serantoni C. R. Fadiga térmica de ferros fundidos brancos multicomponentes. Dissertação de Mestrado. Escola Politécnica da Universidade de São Paulo, 2003.

Tomlinson, W.J., Talks, M. G., Cavitation Erosion of Heat-Treated Low Alloy Cast Irons, Wear, v. 137, 1990, p. 143-146.

7. Responsibility notice

The authors are the only responsible for the printed material included in this paper.